ACS APPLIED MATERIALS & INTERFACES

Research Article

www.acsami.org

High On−Off Ratio Improvement of ZnO-Based Forming-Free Memristor by Surface Hydrogen Annealing

Yihui Sun,[†] Xiaoqin Yan,*[,†] Xin Zheng,[†] Yichong Liu,[†] Yanguang Zhao,[†] Yanwei Shen,[†] Qingliang Liao,[†] and Yue Zhang*[,†,‡]

[†]State Key Laboratory for Advanced Metals and Materials, School of Materials Science and Engineering, University of Science and Technology Beijing, Beijing 100083, People's Republic of China

[‡]Key Laboratory of New Energy Materials and Technologies, University of Science and Technology Beijing, Beijing 100083, People's Republic of China

ABSTRACT: In this work, a high-performance, forming-free memristor based on Au/ZnO nanorods/AZO (Al-doped ZnO conductive glass) sandwich structure has been developed by rapid hydrogen annealing treatment. The R_{on}/R_{off} rate is dramatically increased from ∼10 to ∼10^4 after the surface treatment. Such an enhanced performance is attributed to the introduced oxygen vacancies layer at the top of ZnO nanorods. The device also exhibits excellent switching and retention stability. In addition, the carrier migration behavior can be well interpreted by classical trap-controlled space charge limited conduction, which verifies the forming of conductive filamentary in low resistive state. On this basis, Arrhenius activation theory is adopted to explain the drifting of oxygen vacancies, which is further confirmed by the time pertinence of resistive switching behavior under different sweep speed. This fabrication approach offers a useful approach to enhance the switching properties for next-generation memory applications.

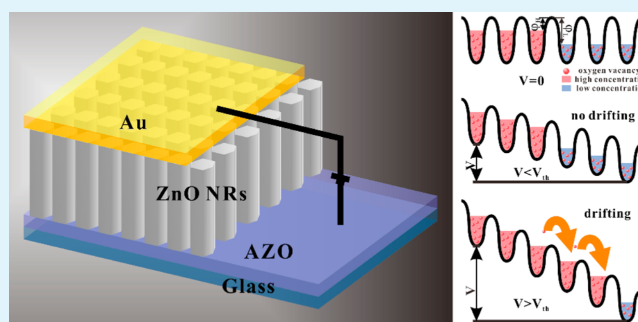

KEYWORDS: *resistive switching, surface hydrogen annealing, forming-free, Arrhenius activation theory, oxygen vacancies drifting*

■ INTRODUCTION

As the fourth fundamental element, the memristor device has attracted broad attention in its applications and operating mechanism since it was discovered by Hewlett-Packard lab in 2008.[1] Resistive switching random access memory (RRAM), as one basic application of memristor, is the most promising candidate to overcome the technological limitations and fulfill the essential requirements for 3-D integrated circuit architecture in the next generation nonvolatile memory.[2−4] It has a high potential to replace current flash memory and dynamic random access memory (DRAM) due to its superior advantages including low power consumption, fast switching speed, excellent cycle stability, and high stacking density.[5]

To further the understanding of its mechanisms, in situ observation of filamentary conducting channels in TiO_2 were realized by high-resolution transmission electron microscopy (TEM).[6] The forming and breakage of conductive filament is the core of resistive switching (RS) behavior. To modulate this point, a series of efforts is made. Some reports explored the influences of various external field, such as an applied magnetic field,[7] temperature,[8] or illumination[9,10] to modulate the memristive switching behavior. The interface-engineering was adopted to improve its performance, for instance, changing the electrode materials,[11] inserting a middle tier between the electrode and oxide,[12] and plugging in the thin layer within the oxide.[13] After intensively investigating the switching mechanisms of RRAM in recent years, the drifting of oxygen vacancies (or oxygen ions) either at the interface or inside of materials under an applied electrical field was demonstrated to play an important role in resistive behavior.[14−16] A large variety of materials, especially metal oxides (WO_x,[17] NiO,[18] and TaO_x[19,20]), have been discovered existing the characteristics of resistive switching. ZnO,[21] containing regulated oxygen vacancies, appears to be one of the most promising materials for its outstanding properties.[22−26] However, there is still an absence of an effective method to enhance the property of memory. Also, a proper theory to explain the drifting of oxygen vacancies is urgently desired.

Here, Au/ZnO nanorods/AZO sandwich structured memristor has been designed. The device exhibited a significant improvement of switch ratio owing to inserting an oxygen vacancies layer when subjected to hydrogen annealing treatment. Superior performance including forming-free characteristic and excellent stability was also obtained. Arrhenius activation theory was further employed to interpret the inner mechanism and matched up well with the time-dependent on resistive switching behavior.

Received: February 4, 2015
Accepted: March 18, 2015
Published: March 18, 2015

ACS Publications © 2015 American Chemical Society

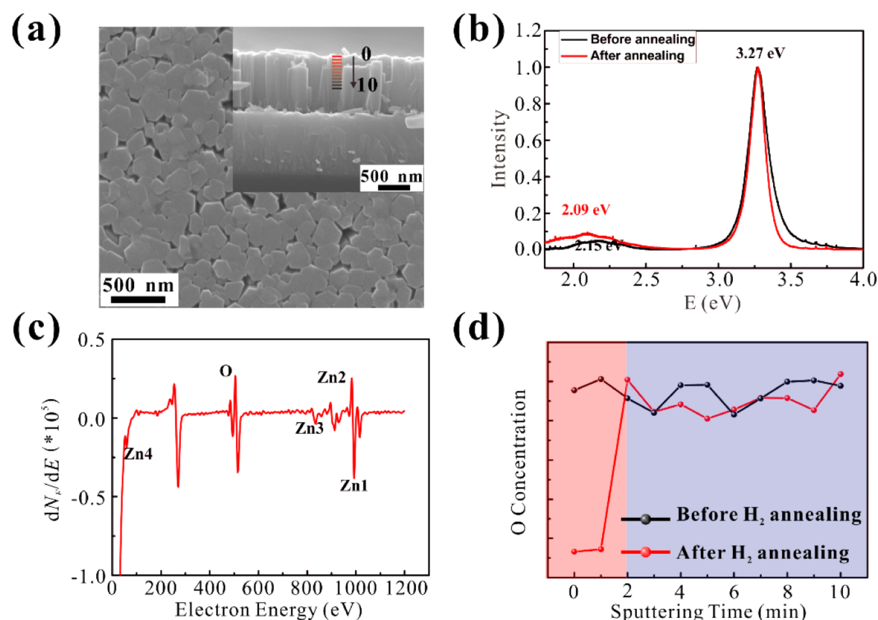

Figure 1. (a) FESEM image of ZnO NRs, the inset is the cross-sectional image; (b) PL spectra of ZnO NRs, before and after H_2 annealing. Parts c and d are the surface auger electron spectroscopy (AES) and AES depth profiles of ZnO NRs, respectively. (d) The pink region is the surface part of ZnO NRs and the blue region is the inner part of ZnO NRs. The number 0−10 in part a is the sputtering time in part d.

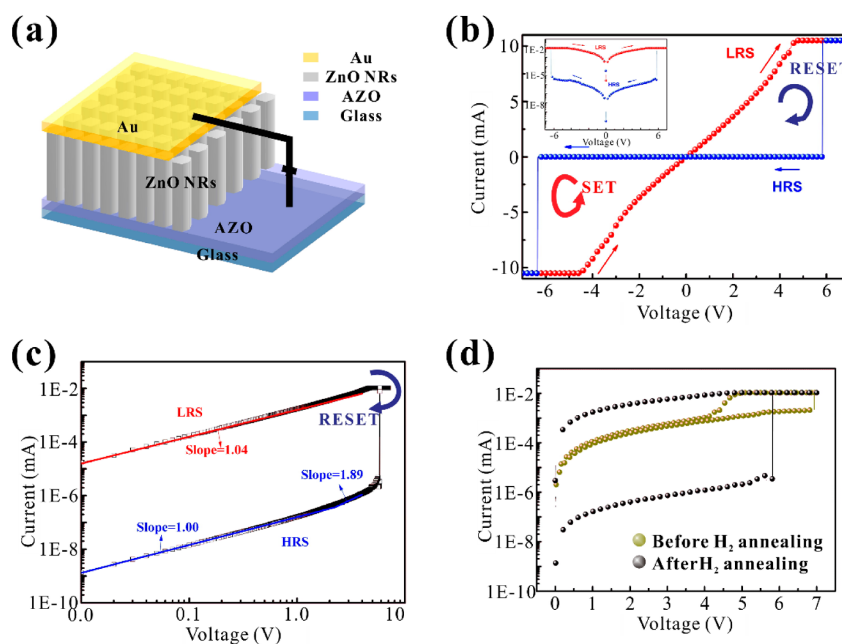

Figure 2. (a) Schematic illustration of Au/ZnO NRs/AZO memristor device; (b) current−voltage ($I-V$) characteristics of the device with annealed ZnO NRs, the inset is the $I-V$ curve in a semilogarithmic scale; (c) logarithmic plot and linear fitting of the $I-V$ curve; (d) comparability circulation $I-V$ curve before and after H_2 annealing.

■ RESULTS AND DISCUSSION

Surface modification has been attempted recently in ZnO-based[8,27] and TiO_2-based[11,28] devices aimed to improve RS characteristics. Low resistive state (LRS) and high resistive state (HRS) distribution can be obtained through surface treatment to provide a controlled RS path. In this paper, rapid surface H_2 annealing significantly decreases the resistance in LRS by introducing large number of oxygen vacancies (V_O) and increases the resistance in HRS by improving the crystallinity in the bottom of ZnO nanorods (NRs). Subsequently, Arrhenius activation theory is applied to account for the V_O drifting process and further confirmed by relevant RS property under various sweep rate.

Figure 1a shows the FESEM image of one-dimensional, high density, and well-aligned ZnO NRs on the AZO glass with an average length of 800 nm and average diameter of 200 nm, respectively. The inset is the sectional view of ZnO NRs. Generally, it is an Ohmic contact between AZO and ZnO NRs, and there is no barrier.[29] So AZO here is just used as the bottom electrode and the seed layer. Oxygen vacancies in ZnO NRs are the key for the property of the memory device. In order to characterize the change of oxygen vacancies

DOI: 10.1021/acsami.5b01080
ACS Appl. Mater. Interfaces 2015, 7, 7382−7388

concentration, the PL spectra of the samples before and after annealing are measured, respectively, as observed in Figure 1b. Both of the spectra have two emission peaks, centering at 3.27 eV (ultraviolet) and ~2.10 eV (green). The UV emission is related to band-edge emission, while the green emission is resulted from the intrinsic defects in ZnO NRs, like oxygen vacancies (V_O).[30,31] Noticeable differences can be found when rapid surface H_2 annealing is adopted: (1) the intensity of defect peak in ZnO NRs PL spectra after annealing is the double of that without annealing. It means H_2 annealing efficiently improves the concentration of oxygen vacancies, which serves as the V_O reservoir; (2) the sharper peak of UV emission with H_2 annealing treatment illustrates better crystallinity in the bottom of nanorods resulting in the higher resistance in HRS. The PL spectra demonstrate that the rapid H_2 annealing treatment has effectively introduced the vacancies-injection-layer and improved the crystallinity in the bottom of NRs, which has a significant impact on the performance of the device.

To get a further insight of oxygen concentration changing caused by H_2 annealing in ZnO NRs, auger electron spectroscopy (AES) depth profiles for the ZnO NRs before and after annealing were surveyed and displayed in parts c and d of Figure 1, respectively. The sputtering rate of the Ar^+ gun was 53 nm/min for SiO_2, which acted as a reference sample. Only the peaks of Zn and O are found in Figure 1c. For researching the inner element distribution, the AES along the depth direction was obtained as depicted in Figure 1d. The concentration of O increases from point 0 to point 3 as illustrated in Figure 1d (red line) and keeps steady from point 3 to point 10. The number expresses the sputtering time as can be seen in Figure 1a, which implies that the H_2 annealing treatment successfully brought in the oxygen vacancies layer at the top of ZnO NRs. By contrast, O concentration keeps stably along the depth direction (black line). The absence of Al (existing in AZO) means all the signals come from ZnO NRs. The AES cannot only verify the existence of the vacancies-injection-layer in the surface but also certify the bilayer with different oxygen vacancies concentration.

The schematic illustration of the Au/ZnO NRs/AZO hybrid structure device is shown in Figure 2a. The two-terminal electrical measurement of ZnO NR-based memory device is conducted across Au electrode and AZO. The current−voltage ($I-V$) characteristics of the Au/ZnO NRs/AZO device with rapid H_2 annealing treatment are illustrated in Figure 2b. The output current of the memristor increases abruptly at ~−6 V, which is defined as the threshold point V_{set}. Another abrupt transition from LRS to HRS occurs at V_{reset}, which is about 6 V. The inset is the $I-V$ curve of the device in a semilogarithmic scale, which can clearly reveal the R_{on}/R_{off} ratio (~10^4) and manifest high performance for memory. The set/reset voltage, compared with the other device, are very large. It is proposed that the large length of ZnO NRs, which is about 800 nm, results in the large set/reset voltage. The relationship between set voltage and length of oxide (d_{oxide}) was surveyed in previous work.[32] The V_{set}/V_{reset} increases with the increase of d_{oxide}. As compliance current has significant impact in the resistive switching behavior,[33] a limited compliance current of 100 mA was adopted to avoid damaging the instrument as previous work[21] during all the measurement. The results of comparison with previous pure-ZnO memristors is illustrated in Table 1. The device in our work has the lowest value in V_{set}/d_{oxide} and pretty good switch ratio. H_2 annealing technology also can be

Table 1. Results of Comparison with Previous Pure-ZnO Memristors

material	V_{set} (V)	V_{reset} (V)	R_{on}/R_{off}	d_{oxide} (nm)	V_{set}/d_{oxide} (V/nm)
ZnO film[35]	1.5	−0.6	$<10^3$	23	6.5/100
ZnO NRs[36]	1.5	−0.8	$<10^2$	150	1.0/100
ZnO nanowire[37]	3.0	−1.6	10^6	250	1.2/100
our work	6.0	−6.0	10^4	800	0.75/100

found in previous work,[34] and 2 orders of magnitude enhancement (from 10 to 10^3) in switch ratio are achieved. Surface hydrogen annealing in our work increases the switch ratio from 10 to 10^4. This high improvement benefits from the controlled resistance state distribution.

To further understand the conduction and switching mechanisms of the memory device, the $I-V$ characteristics were replotted in a log−log scale. Figure 2c demonstrates the logarithmic plot and linear fitting of the $I-V$ curve for the positive voltage sweep region, and they are similar for the negative branch. Obviously, the $I-V$ relationship in LRS exhibits an Ohmic conduction behavior with a slope of 1.04, which is ascribed to the formation of conductive filaments in the device after the SET process. However, the conduction mechanism in HRS is much more complicated. Fitting results for HRS indicate that the charge transport behavior is in good agreement with a classical trap-controlled space charge limited conduction (SCLC).[38] The $I-V$ characteristics in HRS consist of three portions: the Ohmic region ($I \sim V$) with a slope of 1.00 at low bias, the Child's law region ($I \sim V^2$) with a slope of 1.89 at higher bias, and the steep current increase region. The totally different conduction behaviors in LRS and HRS also suggest that the high conductivity in the ON-state device should be resulted from the forming of a confined filamentary. The $I-V$ curves with and without rapid H_2 annealing were measured (Figure 2d). An efficient improvement of R_{on}/R_{off} ratio, from ~10 to ~10^4, was obtained with annealing. Meanwhile, the threshold voltage is reduced from ~7 V to ~6 V. This little decrease is due to annealing that cuts down the length of ZnO NRs in HRS (d_{oxide}). Annealing not only introduced a high-concentration oxygen vacancies layer in the surface of ZnO NRs but also improved the crystallinity in the bottom of the nanorods array. It resulted in the lower resistance in low resistance state (LRS) and the higher resistance in the high resistance state (HRS).

In general, pristine-state oxide materials are too insulative to induce reliable resistive switching due to the low density of defects such as oxygen vacancies or metal interstitials.[39] Therefore, an electroforming process is a prerequisite to operate a device, which is an obstacle for RRAM commercial applications. In the case of the present work, there is a significant amount of oxygen vacancies (V_O) in ZnO NRs due to the H_2 annealing treatment. The detail of oxygen vacancies migration during switch process is presented in Figure 3. As the applied voltage increases from zero and exceeds a threshold voltage of ~−6 V, oxygen vacancies are repelled from the top side of ZnO NRs to the bottom side and form a conductive filament to "turn on" the device, which can be seen in Figure 3a,b. Even if the external bias is removed or reversely polarized to negative values which is lower than the reverse threshold value (V_{reset}), the LRS of the device is still preserved, displaying a nonvolatile nature (Figure 3b). The oxygen vacancies are further attracted from the bottom side to the top side to go

DOI: 10.1021/acsami.5b01080
ACS Appl. Mater. Interfaces 2015, 7, 7382−7388

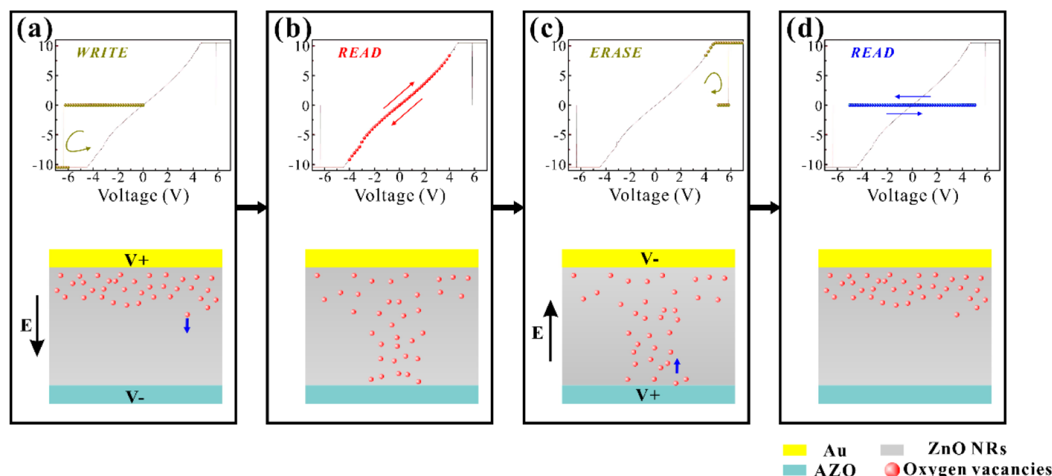

Figure 3. Decomposition diagrams of the switch process. The top panels of parts a, b, c, and d correspond to the process of write, read, erase, and read. The bottom panels shows the schematic diagram of oxygen vacancies drifting in Au/ZnO NRs/AZO devices.

back "off state" causing the breakage of conductive filament once the large-enough positive voltage (~6 V) is applied (Figure 3c). Identically, the applied voltage, below the threshold value (V_{set}), can't change the resistance state, which makes sure the data can be well preserved. The yielded $I-V$ response curves correspond well to memristive switching behavior, indicating that the devices could be reliably written, read, and erased during each step. Both of the switch process and retention process exhibit excellent property, implying a good application prospect for RRAM.

The endurance test of the Au/ZnO NRs/AZO device was also carried out. The stabilities of current and resistance (read at 1 V) are shown in Figure 4a,b accordingly. In the switch process, the current and resistance fluctuated a little when the device circularly transformed between HRS and LRS. It still kept a R_{on}/R_{off} rate of $\sim 10^3$ and the fluctuation mainly appeared in HRS. In the retention process, the applied voltage was swept cyclically between -1 and 1 V in HRS and LRS, respectively, which manifested excellent stability after 80 cycles. That is to say, once the device has achieved LRS (or HRS), it remains in the ON state (or OFF state) during the subsequent voltage scan below the threshold voltage, which is the characteristic of nonvolatile (NV)-type memory. Nonvolatile-type switching behavior is useful in data storage and computing technologies since they allow information to be written to a device, and the data may not be subsequently erased or deleted from the device under a low applied voltage, even if the power is turned off. Moreover, the resistances of the HRS and LRS at a read voltage of 1 V for each process in terms of the cumulative distribution were examined. Clearly, a very narrow distribution of the LRS resistance of $(0.5 \times 10^3)-(1.2 \times 10^3)$ in the switch process (Figure 4c), and a more uniform ratio of R_{HRS}/R_{LRS} could be observed in the retention process (Figure 4d). The device manifests excellent stability for the future use of RRAM.

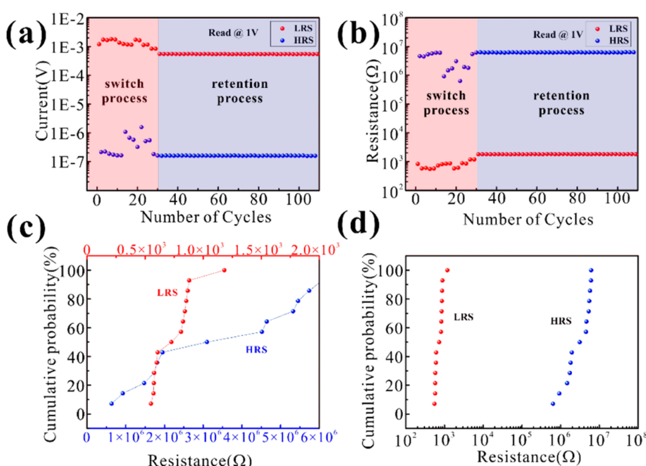

Figure 4. Corresponding endurance tests for current (a) and resistive (b) at a read bias of 0.1 V, respectively. The cumulative distributions of the resistance in switch process (c) and retention process (d).

The schematic of oxygen vacancies drifting is illustrated in Figure 5. φ_L and φ_H are the barrier heights of free oxygen vacancies drifting in low oxygen vacancies concentration and high oxygen vacancies concentration ($\varphi_L \gg \varphi_H$) correspondingly (Figure 5a). The moving of oxygen vacancies needs a driving power larger than "activation energy" to leap over the barrier φ_H, which is furnished by applied voltage. However, it is much more difficult for oxygen vacancies to drift from the low concentration region to the high concentration region for the existence of φ_L. When applying a voltage below the threshold voltage, the driving power is not large enough to drive oxygen vacancies drifting from the high concentration region to the low concentration region (Figure 5b). It's retention process is where the external potential will not change the resistance of the device. In this process, the device can run stably. When applying a voltage beyond the threshold voltage, the driving power is large enough to drive oxygen vacancies drifting from the high concentration region to the low concentration region (Figure 5c). The moving of oxygen vacancies increases its concentration in the low concentration region and decreases the resistance causing the device to transform from HRS to LRS. All the procedures are nonvolatile. This means that the LRS of the device is still preserved even if the external bias is removed or reversely polarized to a negative value which is lower than a threshold value, displaying a nonvolatile nature. The existence of the barrier results in that the oxygen vacancies has no driving power to go back. Meanwhile, the barrier exists not only in the interface but also in the internal, which prevents the free transfer of oxygen vacancies.

We connect this barrier with activation energy in the Arrhenius theory. According to the Arrhenius equation:

DOI: 10.1021/acsami.5b01080
ACS Appl. Mater. Interfaces 2015, 7, 7382−7388

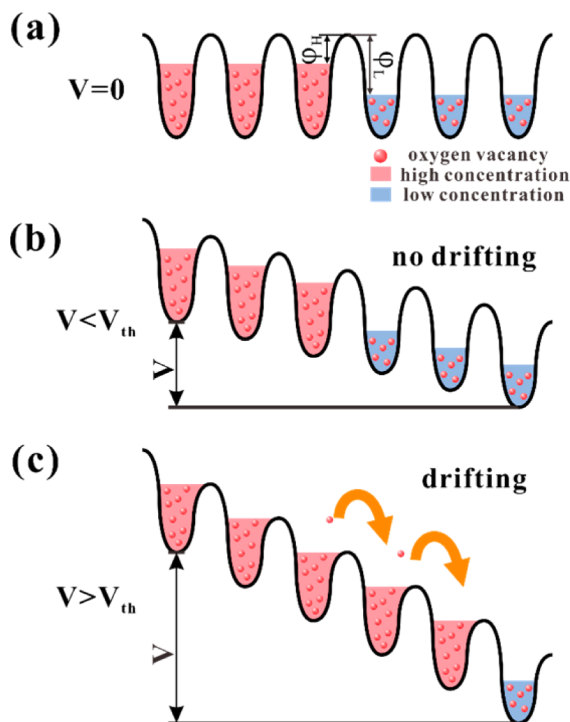

Figure 5. Schematic of oxygen vacancy drifting. (a) There is the barrier to stop the drifting of oxygen vacancies when the applied voltage is zero; (b) the applied voltage isn't large enough to go over the barrier; (c) the applied voltage drives the oxygen vacancies drifting from high concentration to low concentration.

$$\ln K = \ln A - E_a/RT \quad (1)$$

where K is reaction rate constant, A is a pre-exponential factor, E_a is the activation energy, R is the molar gas constant, and T is the thermodynamic temperature.

When it comes to the memristor resistance switch process, eq 1 becomes

$$\ln K_R = \ln A - E_a(V, t)/RT \quad (2)$$

where K_R is the change rate of resistance, and $E_a(V,t)$ is the driving power of oxygen vacancies drifting, which is provided by the applied bias. What should be mentioned is that K_R and $E_a(V,t)$ are parameters related to time (t), which are not referred to in the experiment above. In this theory, the change of resistance is affected by activity energy, environmental temperature, and the applying time which is reflected by K_R and $E_a(V,t)$. The temperature dependence has been certified by previous work.[40] To verify the temporal correlation which exists in K_R and $E_a(V,t)$, the sweep mode is changed to the fast sweep speed mode which leads to different performance (Figure 6).

In the fast sweep speed mode, the device is switched from LRS to HRS in three cycles (Figure 6a). The $I-V$ characteristics of HRS in each cycle were replotted in a log–log scale. Fitting results indicate that the charge transport behavior is in good agreement with SCLC, similar to previous data. Oxygen vacancies move in three cycles from the bottom side to the top side. In the former two loops, the conductive filament becomes thinner and thinner and breaks down in the last loop, resulting in the huge change of resistance. The current has little change when the applied voltage ranges from 0 to 4 V, indicating the existence of "activation energy" which represents the minimum energy to drive oxygen vacancies moving. Meanwhile, the threshold voltage drops to ~5 V in the last cycle, which results from the previous two cycles reducing the activation energy. In the fast sweep speed mode, this device shows evident characters of time cumulation mentioned in eq 2. It will shorten the applied time with changing the sweep mode from normal to fast sweep speed mode which brings about the reduction of external energy $E_a(V,t)$. According to the filament formation model of the thermally activated process,[41] the rate of oxygen vacancies migration ν is determined by the bias-dependent activation energy $E_a(V,t)$

$$\ln \nu = \ln f - E_a(V, t)/k_B T \quad (3)$$

where ν is the rate of oxygen vacancies migration, k_B is Boltzmann's constant, and f is the attempt frequency. Lowering of the apparent activation energy $E_a(V,t)$ by the application of the bias voltage will thus lead to bias-dependent switching rates and wait times. As two important parameters in Arrhenius theory, both of activation energy (correspond to threshold voltage) and time were verified in our experiments, and the similar results could come from different work. All of this above means the Arrhenius theory can be employed properly in resistive switching behavior.

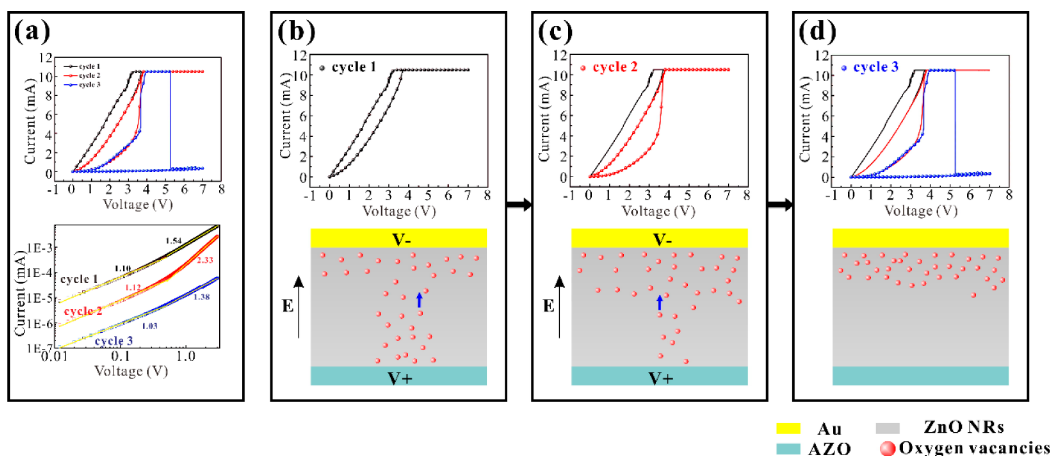

Figure 6. (a) Device switched from LRS to HRS with three cycles in the fast sweep speed mode. The top panels of parts b, c, and d correspond to the first cycle, the second cycle, and the third cycle. The bottom panels show the schematic diagram of oxygen vacancies migration in Au/ZnO NRs/AZO devices.

DOI: 10.1021/acsami.5b01080
ACS Appl. Mater. Interfaces 2015, 7, 7382–7388

CONCLUSIONS

In summary, a novel two-terminal ZnO NRs-based, forming-free memristor has been successfully constructed by utilizing a metal−insulator−metal (MIM) structure. The ZnO NRs were surface-annealed under a hydrogen atmosphere. A thin layer with high concentration of oxygen vacancies was introduced. The thin layer can serve as an oxygen vacancies reservoir, and consequently a large hysteresis loop can been obtained. The R_{on}/R_{off} ratio raised from ∼10 to 10^4 with annealing, which exhibited the characteristic of nonvolatile-type memory. The charge transport behavior was in good agreement with a classical trap-controlled SCLC. Arrhenius theory was applied to explain the existence of threshold voltage which directly reflected the activation energy. The character of time cumulation in resistance transforming was put forward, which matched up with the definition of memristor. Also it was confirmed by simply changing the sweep speed into fast sweep speed mode, which indicated that Arrhenius theory tallied with resistive switching character. Strategies for performance enhancement and the theoretical model proposed here may throw light on its practical application in memory devices.

EXPERIMENTAL SECTION

Fabrication. The aqueous solutions of zinc source (25 mM ($Zn(NO_3)_2$) and alkali source (25 mM hexamethylenetetramine (HMTA)) were prepared, respectively, at room temperature to synthesize ZnO nanorods. Aluminum doped zinc oxide (AZO) film (thickness, ∼900 nm; resistance, ≤10 Ω s q^{-1}; transmittance, ≥80%) were successfully deposited on float glass by radio frequency magnetron sputtering (RFMS) as an electrode and growing substrate. The AZO was cut into small pieces (15 mm × 10 mm) and ultrasonically cleaned in acetone, isopropyl alcohol, and deionized water for 10 min, respectively, subsequently dried using N_2 gas. The substrates were faced downward in a Teflon-lined stainless steel autoclave filled with the aqueous solution and maintained at 95 °C for 4 h. The resulting ZnO NRs were rinsed with DI-water to remove any residual solution. After that, surface annealing treatment was employed in a hydrogen and argon mixture ambience at 350 °C for 15 min to achieve an oxygen vacancies injection layer. The flow rates of hydrogen and argon are 50 and 500 sccm, respectively. The 100 nm-thick Au top electrode was directly deposited on the ZnO NRs by dc sputter at room temperature. During the sputtering, the working pressure was kept at 0.9 Pa and the sputtering time was 120 s. PDMS was used to cover the entire device for protecting it.

Characterization. Field emission scanning electron microscopy (FESEM) (Quanta 3D FEG) with a 20 kV operating voltage was utilized to study the morphologies of the samples. The room temperature photoluminescence spectrum was measured by a Raman spectrometer (Jobin-Yvon, HR800) and excited by a 325 nm He−Cd laser source. The auger electron spectroscopy (ULVAC-PHI 700) with a 5 kV electronic gun voltage was carried out to obtain the concentrations of elements. The electrical properties of the device were performed by a Keithley 4200 testing system with a limited compliance current of 100 mA to avoid damaging the instrument.

AUTHOR INFORMATION

Corresponding Authors

*E-mail: yuezhang@ustb.edu.cn. Phone: +86 10 62334725. Fax: +86 10 62332011.
*E-mail: xqyan@mater.ustb.edu.cn. Phone: +86 10 62334725. Fax: +86 10 62332011.

Notes

The authors declare no competing financial interest.

ACKNOWLEDGMENTS

This work was supported by the National Major Research Program of China (Grant 2013CB932602), the Major Project of International Cooperation and Exchanges (Grant 2012DFA50990), the Program of Introducing Talents of Discipline to Universities, NSFC (Grants 51232001, 51172022, 51372023, and 51372020), the Research Fund of Co-construction Program from Beijing Municipal Commission of Education, the Fundamental Research Funds for the Central Universities, and the Program for Changjiang Scholars and Innovative Research Team in University.

REFERENCES

(1) Strukov, D. B.; Snider, G. S.; Stewart, D. R.; Williams, R. S. The missing memristor found. *Nature* **2008**, *453* (7191), 80−83.
(2) Linn, E.; Rosezin, R.; Kugeler, C.; Waser, R. Complementary resistive switches for passive nanocrossbar memories. *Nat. Mater.* **2010**, *9* (5), 403−406.
(3) Yang, J. J.; Borghetti, J.; Murphy, D.; Stewart, D. R.; Williams, R. S. A Family of Electronically Reconfigurable Nanodevices. *Adv. Mater.* **2009**, *21* (37), 3754−3758.
(4) He, L.; Liao, Z. M.; Wu, H. C.; Tian, X. X.; Xu, D. S.; Cross, G. L.; Duesberg, G. S.; Shvets, I. V.; Yu, D. P. Memory and threshold resistance switching in Ni/NiO core-shell nanowires. *Nano Lett.* **2011**, *11* (11), 4601−4606.
(5) Kim, S.; Jeong, H. Y.; Kim, S. K.; Choi, S. Y.; Lee, K. J. Flexible memristive memory array on plastic substrates. *Nano Lett.* **2011**, *11* (12), 5438−5442.
(6) Yang, Y.; Gao, P.; Gaba, S.; Chang, T.; Pan, X.; Lu, W. Observation of conducting filament growth in nanoscale resistive memories. *Nat. Commun.* **2012**, *3*, 732.
(7) Wang, X. L.; Shao, Q.; Leung, C. W.; Lortz, R.; Ruotolo, A. Non-volatile, electric control of magnetism in Mn-substituted ZnO. *Appl. Phys. Lett.* **2014**, *104* (6), 062409.
(8) Lin, S. M.; Huang, J. S.; Chang, W. C.; Hou, T. C.; Huang, H. W.; Huang, C. H.; Lin, S. J.; Chueh, Y. L. Single-step formation of ZnO/ZnWO(x) bilayer structure via interfacial engineering for high performance and low energy consumption resistive memory with controllable high resistance states. *ACS Appl. Mater. Interfaces* **2013**, *5* (16), 7831−7837.
(9) Hu, W.; Zou, L.; Chen, X.; Qin, N.; Li, S.; Bao, D. Highly uniform resistive switching properties of amorphous InGaZnO thin films prepared by a low temperature photochemical solution deposition method. *ACS Appl. Mater. Interfaces* **2014**, *6* (7), 5012−5017.
(10) Park, J.; Lee, S.; Lee, J.; Yong, K. A light incident angle switchable ZnO nanorod memristor: reversible switching behavior between two non-volatile memory devices. *Adv. Mater.* **2013**, *25* (44), 6423−6429.
(11) Jeong, H. Y.; Lee, J. Y.; Choi, S. Y. Interface-Engineered Amorphous TiO2-Based Resistive Memory Devices. *Adv. Funct. Mater.* **2010**, *20* (22), 3912−3917.
(12) Park, W. I.; Yoon, J. M.; Park, M.; Lee, J.; Kim, S. K.; Jeong, J. W.; Kim, K.; Jeong, H. Y.; Jeon, S.; No, K. S.; Lee, J. Y.; Jung, Y. S. Self-assembly-induced formation of high-density silicon oxide memristor nanostructures on graphene and metal electrodes. *Nano Lett.* **2012**, *12* (3), 1235−1240.
(13) Yang, J. J.; Pickett, M. D.; Li, X.; Ohlberg, D. A.; Stewart, D. R.; Williams, R. S. Memristive switching mechanism for metal/oxide/metal nanodevices. *Nat. Nanotechnol* **2008**, *3* (7), 429−433.
(14) Waser, R.; Aono, M. Nanoionics-based resistive switching memories. *Nat. Mater.* **2007**, *6* (11), 833−840.
(15) Chang, S. H.; Lee, J. S.; Chae, S. C.; Lee, S. B.; Liu, C.; Kahng, B.; Kim, D. W.; Noh, T. W. Occurrence of Both Unipolar Memory and Threshold Resistance Switching in a NiO Film. *Phys. Rev. Lett.* **2009**, *102* (2), 026801.

DOI: 10.1021/acsami.5b01080
ACS Appl. Mater. Interfaces 2015, 7, 7382−7388

(16) Driscoll, T.; Kim, H. T.; Chae, B. G.; Kim, B. J.; Lee, Y. W.; Jokerst, N. M.; Palit, S.; Smith, D. R.; Di Ventra, M.; Basov, D. N. Memory metamaterials. *Science* **2009**, *325* (5947), 1518−1521.

(17) Bai, Y.; Wu, H. Q.; Zhang, Y.; Wu, M. H.; Zhang, J. Y.; Deng, N.; Qian, H.; Yu, Z. P. Low power W:AlOx/WOx bilayer resistive switching structure based on conductive filament formation and rupture mechanism. *Appl. Phys. Lett.* **2013**, *102* (17), 173503.

(18) Panda, D.; Dhar, A.; Ray, S. K. Nonvolatile and unipolar resistive switching characteristics of pulsed laser ablated NiO films. *J. Appl. Phys.* **2010**, *108* (10), 104513.

(19) Miao, F.; Yi, W.; Goldfarb, I.; Yang, J. J.; Zhang, M. X.; Pickett, M. D.; Strachan, J. P.; Medeiros-Ribeiro, G.; Williams, R. S. Continuous electrical tuning of the chemical composition of TaO(x)-based memristors. *ACS Nano* **2012**, *6* (3), 2312−2318.

(20) Park, G. S.; Kim, Y. B.; Park, S. Y.; Li, X. S.; Heo, S.; Lee, M. J.; Chang, M.; Kwon, J. H.; Kim, M.; Chung, U. I.; Dittmann, R.; Waser, R.; Kim, K. In situ observation of filamentary conducting channels in an asymmetric Ta(2)O5-x/TaO2-x bilayer structure. *Nat. Commun.* **2013**, *4*, 2382.

(21) Yang, Y. C.; Pan, F.; Liu, Q.; Liu, M.; Zeng, F. Fully room-temperature-fabricated nonvolatile resistive memory for ultrafast and high-density memory application. *Nano Lett.* **2009**, *9* (4), 1636−1643.

(22) Yang, Y.; Guo, W.; Wang, X.; Wang, Z.; Qi, J.; Zhang, Y. Size dependence of dielectric constant in a single pencil-like ZnO nanowire. *Nano Lett.* **2012**, *12* (4), 1919−1922.

(23) Su, J.; Li, H.; Huang, Y.; Xing, X.; Zhao, J.; Zhang, Y. Electronic transport properties of In-doped ZnO nanobelts with different concentration. *Nanoscale* **2011**, *3* (5), 2182−2187.

(24) Zhang, Y.; Yan, X.; Yang, Y.; Huang, Y.; Liao, Q.; Qi, J. Scanning probe study on the piezotronic effect in ZnO nanomaterials and nanodevices. *Adv. Mater.* **2012**, *24* (34), 4647−4655.

(25) Huang, Y.; Zhang, Y.; Wang, X.; Bai, X.; Gu, Y.; Yan, X.; Liao, Q.; Qi, J.; Liu, J. Size Independence and Doping Dependence of Bending Modulus in ZnO Nanowires. *Cryst. Growth Des.* **2009**, *9* (4), 1640−1642.

(26) Zhang, X.-M.; Lu, M.-Y.; Zhang, Y.; Chen, L.-J.; Wang, Z. L. Fabrication of a High-Brightness Blue-Light-Emitting Diode Using a ZnO-Nanowire Array Grown on p-GaN Thin Film. *Adv. Mater.* **2009**, *21* (27), 2767−2770.

(27) Huang, T. H.; Yang, P. K.; Lien, D. H.; Kang, C. F.; Tsai, M. L.; Chueh, Y. L.; He, J. H. Resistive memory for harsh electronics: immunity to surface effect and high corrosion resistance via surface modification. *Sci. Rep.* **2014**, *4*, 4402.

(28) Bae, Y. C.; Lee, A. R.; Lee, J. B.; Koo, J. H.; Kwon, K. C.; Park, J. G.; Im, H. S.; Hong, J. P. Oxygen Ion Drift-Induced Complementary Resistive Switching in Homo TiOx/TiOy/TiOx and Hetero TiOx/TiON/TiOx Triple Multilayer Frameworks. *Adv. Funct. Mater.* **2012**, *22* (4), 709−716.

(29) Chen, X.; Lin, P.; Yan, X.; Bai, Z.; Yuan, H.; Shen, Y.; Liu, Y.; Zhang, G.; Zhang, Z.; Zhang, Y. Three-Dimensional Ordered ZnO/Cu2O Nanoheterojunctions for Efficient Metal-Oxide Solar Cells. *ACS Appl. Mater. Interfaces* **2015**, *7* (5), 3216−3223.

(30) Zeng, H. B.; Duan, G. T.; Li, Y.; Yang, S. K.; Xu, X. X.; Cai, W. P. Blue Luminescence of ZnO Nanoparticles Based on Non-Equilibrium Processes: Defect Origins and Emission Controls. *Adv. Funct. Mater.* **2010**, *20* (4), 561−572.

(31) Vanheusden, K.; Seager, C. H.; Warren, W. L.; Tallant, D. R.; Voigt, J. A. Correlation between photoluminescence and oxygen vacancies in ZnO phosphors. *Appl. Phys. Lett.* **1996**, *68* (3), 403.

(32) Kim, S.; Choi, S.; Lee, J.; Lu, W. D. Tuning Resistive Switching Characteristics of Tantalum Oxide Memristors through Si Doping. *ACS Nano* **2014**, *8* (10), 10262−10269.

(33) Sowinska, M.; Bertaud, T.; Walczyk, D.; Thiess, S.; Calka, P.; Alff, L.; Walczyk, C.; Schroeder, T. In-operando hard X-ray photoelectron spectroscopy study on the impact of current compliance and switching cycles on oxygen and carbon defects in resistive switching Ti/HfO2/TiN cells. *J. Appl. Phys.* **2014**, *115* (20), 204509.

(34) Kim, H.-D.; An, H.-M.; Kim, T. G. Improved reliability of Au/Si(3)N(4)/Ti resistive switching memory cells due to a hydrogen postannealing treatment. *J. Appl. Phys.* **2011**, *109* (1), 016105.

(35) Lee, S.; Kim, H.; Yun, D. J.; Rhee, S. W.; Yong, K. Resistive switching characteristics of ZnO thin film grown on stainless steel for flexible nonvolatile memory devices. *Appl. Phys. Lett.* **2009**, *95* (26), 262113.

(36) Huang, C. H.; Huang, J. S.; Lin, S. M.; Chang, W. Y.; He, J. H.; Chueh, Y. L. ZnO1-x nanorod arrays/ZnO thin film bilayer structure: from homojunction diode and high-performance memristor to complementary 1D1R application. *ACS Nano* **2012**, *6* (9), 8407−8414.

(37) Yang, Y.; Zhang, X.; Gao, M.; Zeng, F.; Zhou, W.; Xie, S.; Pan, F. Nonvolatile resistive switching in single crystalline ZnO nanowires. *Nanoscale* **2011**, *3* (4), 1917−1921.

(38) Lampert, M. Simplified Theory of Space-Charge-Limited Currents in an Insulator with Traps. *Phys. Rev.* **1956**, *103* (6), 1648−1656.

(39) Yang, J. J.; Inoue, I. H.; Mikolajick, T.; Hwang, C. S. Metal oxide memories based on thermochemical and valence change mechanisms. *MRS Bull.* **2012**, *37* (2), 131−137.

(40) Choi, S.; Yang, Y.; Lu, W. Random telegraph noise and resistance switching analysis of oxide based resistive memory. *Nanoscale* **2014**, *6* (1), 400−404.

(41) Jo, S. H.; Kim, K. H.; Lu, W. Programmable resistance switching in nanoscale two-terminal devices. *Nano Lett.* **2009**, *9* (1), 496−500.

DOI: 10.1021/acsami.5b01080
ACS Appl. Mater. Interfaces 2015, 7, 7382−7388